Visible-Light-Induced Reversible Photomagnetism in Rubidium Manganese Hexacyanoferrate

Hiroko Tokoro,[†,‡,||] Tomoyuki Matsuda,[†] Tomohiro Nuida,[†] Yutaka Moritomo,[§] Kenji Ohoyama,[△] Edgard Davy Loutete Dangui,[⊥] Kamel Boukheddaden,[⊥] and Shin-ichi Ohkoshi*[,†]

Departments of Chemistry and of Physics, School of Science, The University of Tokyo, 7-3-1 Hongo, Bunkyo-ku, Tokyo, 113-0033 Japan, Department of Physics, School of Pure and Applied Science, University of Tsukuba, 1-1-1 Tenodai, Tsukuba, Ibaraki, 305-8571 Japan, Institute for Materials Research, Tohoku University, 2-1-1 Katahira, Aoba-ku, Sendai, Miyagi, 980-8577 Japan, and Groupe d'Etudes de la Matière Condensée, CNRS Université de Versailles St. Quentin en Yvelines, 45 Avenue des États Unis, F78035 Versailles Cedex, France

Received July 17, 2007. Revised Manuscript Received October 17, 2007

The photoreversibility of a photoinduced phase transition was investigated in a rubidium manganese hexacyanoferrate, $Rb_{0.88}Mn[Fe(CN)_6]_{0.96}\cdot 0.5H_2O$. The present material shows a charge-transfer phase transition from the $Mn^{II}-Fe^{III}$ [high-temperature (HT)] phase to the $Mn^{III}-Fe^{II}$ [low-temperature (LT)] phase, and the LT phase shows ferromagnetism. Spectroscopic ellipsometry measurements of the dielectric constant suggest that the optical transitions in the LT and HT phases are a metal-to-metal charge transfer ($Fe^{II} \rightarrow Mn^{III}$) band at 420–540 nm and a ligand-to-metal charge transfer ($CN^- \rightarrow Fe^{III}$) band of $[Fe^{III}(CN)_6]$ at 410 nm, respectively. By irradiation with 532 nm light, the LT phase is transmitted to the photoinduced (PI) phase, which has a valence state similar to that of the HT phase, and photodemagnetization is observed. In contrast, irradiating the PI phase with 410 ± 30 nm light causes the reverse phase transition. Neutron powder diffraction measurement of an analogue compound, $Rb_{0.58}Mn[Fe(CN)_6]_{0.86}\cdot 2.3H_2O$, which does not show a charge-transfer phase transition and maintains the $Mn^{II}-Fe^{III}$ phase at a very low temperature, confirms that the PI phase is an antiferromagnet. Hence, the present visible-light-induced reversible photomagnetic effect is due to optical switching between the ferromagnetic LT phase and the antiferromagnetic PI phase.

1. Introduction

One challenge in the field of molecule-based magnets is to develop novel optofunctionalities such as photomagnetism,[1–19] a magnetooptical effect,[20–22] and a nonlinear magnetooptical effect.[23,24] Photoinduced magnetization has been observed in several cyano-bridged metal complexes such as cobalt hexacyanoferrate,[4] cobalt octacyanotungstate,[10–12] and copper octacyanomolybdate.[13–17] One possible route to optically control magnetization is to change the electronic spin state of a magnetic material. The bistability of the electronic states is also important for observing a persistent photoinduced state because the energy barrier between these bistable states

* Corresponding author. E-mail: ohkoshi@chem.s.u-tokyo.ac.jp. Tel: +81-3-5841-4331. Fax: +81-3-3812-1896.
[†] Department of Chemistry, School of Science, The University of Tokyo.
[‡] Department of Physics, School of Science, The University of Tokyo.
[§] University of Tsukuba.
[△] Tohoku University.
[⊥] CNRS Université de Versailles St. Quentin en Yvelines.
[||] PRESTO, JST, 4-1-8 Honcho Kawaguchi, Saitama, Japan.

(1) Dei, A. *Angew. Chem., Int. Ed.* **2005**, *44*, 1160.
(2) Verdaguer, M. *Science* **1996**, *272*, 698.
(3) Ohkoshi, S.; Hashimoto, K. *J. Photochem. Photobiol. C* **2001**, *2*, 71.
(4) Sato, O.; Hayami, S.; Einaga, Y.; Gu, Z. Z. *Bull. Chem. Soc. Jpn.* **2003**, *76*, 443.
(5) Ohkoshi, S.; Yorozu, S.; Sato, O.; Iyoda, T.; Fujishima, A.; Hashimoto, K. *Appl. Phys. Lett.* **1997**, *70*, 1040.
(6) Ohkoshi, S.; Hashimoto, K. *J. Am. Chem. Soc.* **1999**, *121*, 10591.
(7) Pejaković, D. A.; Manson, J. L.; Miller, J. S.; Epstein, A. J. *Phys. Rev. Lett.* **2000**, *85*, 1994.
(8) Bleuzen, A.; Lomenech, C.; Escax, V.; Villain, F.; Varret, F.; Moulin, C. C.; Verdaguer, M. *J. Am. Chem. Soc.* **2000**, *122*, 6648.
(9) Moore, J. G.; Lochner, E. J.; Ramsey, C.; Dalal, N. S.; Stiegman, A. E. *Angew. Chem., Int. Ed.* **2003**, *42*, 2741.
(10) Arimoto, Y.; Ohkoshi, S.; Zhong, Z. J.; Seino, H.; Mizobe, Y.; Hashimoto, K. *J. Am. Chem. Soc.* **2003**, *125*, 9240.
(11) Le Bris, R.; Mathonière, C.; Létard, J. F. *Chem. Phys. Lett.* **2006**, *426*, 380.
(12) Ohkoshi, S.; Ikeda, S.; Hozumi, T.; Kashiwagi, T.; Hashimoto, K. *J. Am. Chem. Soc.* **2006**, *128*, 5320.
(13) Ohkoshi, S.; Machida, N.; Zhong, Z. J.; Hashimoto, K. *Synth. Met.* **2001**, *122*, 523.
(14) Rombaut, G.; Verelst, M.; Golhen, S.; Ouahab, L.; Mathonière, C.; Kahn, O. *Inorg. Chem.* **2001**, *40*, 1151.
(15) Herrera, J. M.; Marvaud, V.; Verdaguer, M.; Marrot, J.; Kalisz, M.; Mathonière, C. *Angew. Chem., Int. Ed.* **2004**, *43*, 5468.
(16) Ohkoshi, S.; Tokoro, H.; Hozumi, T.; Zhang, Y.; Hashimoto, K.; Mathonière, C.; Bord, I.; Rombaut, G.; Verelst, M.; Moulin, C. C.; Villain, F. *J. Am. Chem. Soc.* **2006**, *128*, 270.
(17) Brinzei, D.; Catala, L.; Mathonière, C.; Wernsdorfer, W.; Gloter, A.; Stephan, O.; Mallah, T. *J. Am. Chem. Soc.* **2007**, *129*, 3778.
(18) Bénard, S.; Rivière, E.; Yu, P. *Chem. Mater.* **2001**, *13*, 159.
(19) Pejaković, D. A.; Kitamura, C.; Miller, J. S.; Epstein, A. J. *Phys. Rev. Lett.* **2002**, *88*, 057202.
(20) Ohkoshi, S.; Mizuno, M.; Hung, G. J.; Hashimoto, K. *J. Phys. Chem. B* **2000**, *104*, 9366.
(21) Andreés, R.; Brissard, M.; Gruselle, M.; Train, C.; Vaissermann, J.; Malézieux, B.; Jamet, J. P.; Verdaguer, M. *Inorg. Chem.* **2001**, *40*, 4633.
(22) Kaneko, W.; Ohba, M.; Ohkawa, H.; Kitagawa, S. *Inorg. Chem.* **2006**, *45*, 7191.
(23) Aktsipetrov, O. A.; Braginskii, O. V.; Esikov, D. A. *Sov. J. Quantum Electron.* **1990**, *20*, 259.
(24) Ikeda, K.; Ohkoshi, S.; Hashimoto, K. *Chem. Phys. Lett.* **2001**, *349*, 371.

10.1021/cm701873s CCC: $40.75
Published on Web 12/19/2007

maintains a photoproduced state even after photoirradiation is terminated. From this viewpoint, a rubidium manganese hexacyanoferrate, which is a Prussian blue analogue,[25–38] is a suitable system. Compounds in this series show a charge-transfer phase transition from $Mn^{II}(S = {}^5/_2)-NC-Fe^{III}(S = {}^1/_2)$ [high-temperature (HT) phase] to $Mn^{III}(S = 2)-NC-Fe^{II}(S = 0)$ [low-temperature (LT) phase].[39,40] This charge-transfer phase transition is accompanied by a structural change from a cubic to a tetragonal structure due to Jahn–Teller distortion of Mn^{III}. The LT phase shows ferromagnetism due to the ferromagnetic coupling between Mn^{III} spins, and the spin ordering has been confirmed by the neutron diffraction pattern and theoretical calculations.[41,42] Moreover, some interesting functionalities have been observed within this series,[43–47] e.g., a magnetization-induced second-harmonic generation, an X-ray-induced phase transition, a pressure-induced magnetic pole inversion, and a ferroelectric ferromagnetism. In our previous paper, we have reported that irradiating with 532 nm light converts the LT phase to the photoinduced (PI) phase, which decreases its spontaneous magnetization.[48] In our current study, we have found that irradiating with a different wavelength of light recovers the PI phase in $Rb_{0.88}Mn[Fe(CN)_6]_{0.96}\cdot 0.5H_2O$ to the LT phase. Furthermore, neutron powder diffraction using an analogue complex, $Rb_{0.58}Mn[Fe(CN)_6]_{0.86}\cdot 2.3H_2O$, has confirmed the magnetic ordering of the PI phase. Herein, we report the dielectric constant (ϵ) for the LT and HT phases measured by spectroscopic ellipsometry, the visible-light-induced reversible changes in the electronic and magnetic properties of $Rb_{0.88}Mn[Fe(CN)_6]_{0.96}\cdot 0.5H_2O$, the neutron powder diffraction pattern of $Rb_{0.58}Mn[Fe(CN)_6]_{0.86}\cdot 2.3H_2O$, and the mechanism of the observed photoreversible photomagnetism.

2. Experimental Section

Compounds. $Rb_{0.88}Mn[Fe(CN)_6]_{0.96}\cdot 0.5H_2O$ was prepared using a modified method from our previous report.[40] An aqueous solution of $MnCl_2$ (0.1 mol dm^{-3}) was reacted with a mixed aqueous solution of RbCl (0.6 mol dm^{-3}) and $K_3[Fe(CN)_6]$ (0.1 mol dm^{-3}). The mixed solution was then stirred at 40 °C, and the precipitate was filtered. Elemental analyses for Rb, Mn, and Fe were performed by an HP4500 inductively coupled plasma mass spectrometer, while those for C, H, and N were performed by standard microanalytical methods. Elemental analyses of the prepared sample showed that the formula was $Rb_{0.88}Mn[Fe(CN)_6]_{0.96}\cdot 0.5H_2O$. Calcd: Rb, 21.95; Mn, 16.03; Fe, 15.65; C, 20.19; N, 23.55. Found: Rb, 21.96; Mn, 16.15; Fe, 15.63; C, 19.83; N, 23.79.

$Rb_{0.58}Mn[Fe(CN)_6]_{0.86}\cdot 2.3H_2O$ for the neutron powder diffraction measurement was prepared by reacting an aqueous solution (0.1 mol dm^{-3}) of $MnCl_2$ with a mixed aqueous solution of RbCl (0.1 mol dm^{-3}) and $K_3[Fe(CN)_6]$ (0.1 mol dm^{-3}). Elemental analyses of the sample showed that the formula was $Rb_{0.58}Mn[Fe(CN)_6]_{0.86}\cdot 2.3H_2O$. Calcd: Rb, 15.10; Mn, 16.74; Fe, 14.63; C, 18.88; N, 22.02. Found; Rb, 15.36; Mn, 16.46; Fe, 14.63; C, 18.99; N, 22.34.

Measurements. The ϵ value between 350 and 800 nm was measured by spectroscopic ellipsometry using a J. A. Woollam variable-angle spectroscopic ellipsometer and a powder sample pressed under 4×10^3 kg cm^{-2} into a pellet. The optical spectra of the irradiation lights were measured by a Hamamatsu Photonics photonic multichannel analyzer PMA-12. Infrared (IR) spectra were recorded on a Shimadzu FT-IR 8200PC spectrometer using CaF_2 plates. The temperature during the IR measurements was controlled by an Oxford Instruments MICROSTATE–He. The magnetic properties were measured using a superconducting quantum interference device (SQUID) magnetometer (Quantum Design MPMS-XL). The sample was supported on commercial transparent adhesive tape, which was placed on the edge of an optical fiber. For the light irradiation experiment, a green light ($\lambda = 532$ nm, 30 mW cm^{-2}) with a continuous-wave (CW) diode laser, a blue light ($\lambda = 410 \pm 30$ nm, 13 mW cm^{-2}), and a blue-green light ($\lambda = 425 \pm 45$ nm, 22 mW cm^{-2}) of a filtered xenon lamp were used as the irradiating light sources. Neutron powder diffraction measurements were performed using a Kinken powder diffractometer for the high-efficiency and high-resolution measurements (HERMES) of the Institute for Materials Research, Tohoku University, installed in the JRR-3 M reactor at the Japan Atomic Energy Research Institute, Tokai, Japan. Neutrons with wavelengths of 1.8207 Å were obtained by the 331 reflections of the Ge monochromator and 12-B-Sample-18 collimation. The powder sample was sealed in a vanadium capsule (9 mm diameter) with helium gas and mounted at the cold head of a closed-cycle helium-gas refrigerator. The diffraction data were integrated for 14 h. The crystal and magnetic structures were analyzed by the Rietveld program (*RIETAN-FP*[49]).

3. Results and Discussion

3.1. Visible-Light-Induced Reversible Photomagnetism in $Rb_{0.88}Mn[Fe(CN)_6]_{0.96}\cdot 0.5H_2O$.

Electronic States and

(25) Ludi, A.; Güdel, H. U. *Struct. Bonding (Berlin)* **1973**, 141.
(26) Verdaguer, M.; Mallah, T.; Gadet, V.; Castro, I.; Hélary, C.; Thiébaut, S.; Veillet, P. *Conf. Coord. Chem.* **1993**, *14*, 19.
(27) Ferlay, S.; Mallah, T.; Ouahès, R.; Veillet, P.; Verdaguer, M. *Nature* **1995**, *378*, 701.
(28) Entley, W. R.; Girolami, G. S. *Science* **1995**, *268*, 397.
(29) Ohkoshi, S.; Abe, Y.; Fujishima, A.; Hashimoto, K. *Phys. Rev. Lett.* **1999**, *82*, 1285.
(30) Holmes, S. M.; Girolami, G. S. *J. Am. Chem. Soc.* **1999**, *121*, 5593.
(31) Hatlevik, Ø.; Buschmann, W. E.; Zhang, J.; Manson, J. L.; Miller, J. S. *Adv. Mater.* **1999**, *11*, 914.
(32) Ohkoshi, S.; Arai, K.; Sato, Y.; Hashimoto, K. *Nat. Mater.* **2004**, *3*, 857.
(33) Margadonna, S.; Prassides, K.; Fitch, A. N. *J. Am. Chem. Soc.* **2004**, *126*, 15390.
(34) Goodwin, A. L.; Chapman, K. W.; Kepert, C. J. *J. Am. Chem. Soc.* **2005**, *127*, 17980.
(35) Kaye, S. S.; Long, J. R. *J. Am. Chem. Soc.* **2005**, *127*, 6506.
(36) Miyashita, S.; Konishi, Y.; Tokoro, H.; Nishino, M.; Boukheddaden, K.; Varret, F. *Prog. Theor. Phys.* **2005**, *114*, 719.
(37) Boukheddaden, K.; Nishino, M.; Miyashita, M.; Varret, F. *Phys. Rev. B* **2005**, *72*, 14467.
(38) Berlinguette, C. P.; Dragulescu-Andrasi, A.; Sieber, A.; Güdel, H. U.; Achim, C.; Dunbar, K. R. *J. Am. Chem. Soc.* **2005**, *127*, 6766.
(39) Ohkoshi, S.; Tokoro, H.; Utsunomiya, M.; Mizuno, M.; Abe, M.; Hashimoto, K. *J. Phys. Chem. B* **2002**, *106*, 2423.
(40) Tokoro, H.; Ohkoshi, S.; Matsuda, T.; Hashimoto, K. *Inorg. Chem.* **2004**, *43*, 5231.
(41) Moritomo, Y.; Kuriki, A.; Ohoyama, K.; Tokoro, H.; Ohkoshi, S.; Hashimoto, K.; Hamada, N. *J. Phys. Soc. Jpn.* **2003**, *72*, 456.
(42) Kato, K.; Moritomo, Y.; Sakata, M.; Umekawa, M; Hamada, N.; Ohkoshi, S.; Tokoro, H.; Hashimoto, K. *Phys. Rev. Lett.* **2003**, *91*, 255502.
(43) Margadonna, S.; Prassides, K.; Fitch, A. N. *Angew. Chem., Int. Ed.* **2004**, *43*, 6316.
(44) Ohkoshi, S.; Nuida, T.; Matsuda, T.; Tokoro, H.; Hashimoto, K. *J. Mater. Chem.* **2005**, *15*, 3291.
(45) Nuida, T.; Matsuda, T.; Tokoro, H.; Sakurai, S.; Hashimoto, K.; Ohkoshi, S. *J. Am. Chem. Soc.* **2005**, *127*, 11604.
(46) Egan, L.; Kamenev, K.; Papanikolaou, D.; Takabayashi, Y.; Margadonna, S. *J. Am. Chem. Soc.* **2006**, *128*, 6034.
(47) Ohkoshi, S.; Tokoro, H.; Matsuda, T.; Takahashi, H.; Irie, H.; Hashimoto, K. *Angew. Chem., Int. Ed.* **2007**, *46*, 3238.
(48) Tokoro, H.; Ohkoshi, S.; Hashimoto, K. *Appl. Phys. Lett.* **2003**, *82*, 1245.
(49) Izumi, F.; Ikeda, T. *Mater. Sci. Forum* **2000**, *198*, 321.

Crystal Structures of the LT and HT Phases. The prepared compound was a light-brown powder. The temperature dependence of the molar magnetic susceptibility (χ_M) indicated that the compound exhibited a thermal phase transition between the HT and LT phases with transition temperatures of 222 K ($=T_{1/2\downarrow}$: HT → LT phases) and 298 K ($= T_{1/2\uparrow}$: LT → HT phases) (Figure S1a of the Supporting Information). The temperature dependence in the IR spectra indicated that the valence states of the HT and LT phases were $Rb^{I}_{0.88}Mn^{II}[Fe^{III}(CN)_6]_{0.96}\cdot 0.5H_2O$ and $Rb^{I}_{0.88}Mn^{II}_{0.04}Mn^{III}_{0.96}[Fe^{II}(CN)_6]_{0.96}\cdot 0.5H_2O$, respectively (Figure S1b of the Supporting Information). The temperature dependence of the X-ray diffraction (XRD) patterns showed that the structure of the HT phase was cubic ($F\bar{4}3m$) with a lattice constant of $a = 10.547(7)$ Å at 300 K, while that of the LT phase was tetragonal ($I\bar{4}m2$) with a and $b = 7.099(2)$ Å and $c = 10.568(5)$ Å at 100 K (Figure S1c of the Supporting Information).

ϵ Spectra of the LT and HT Phases. Spectroscopic ellipsometry was used to measure the ϵ spectra in the visible region and to assign the electronic transitions for the LT and HT phases of $Rb_{0.88}Mn[Fe(CN)_6]_{0.96}\cdot 0.5H_2O$. The LT phase was obtained by slow cooling to 160 K using N_2 vapor and then measurement of ϵ at 275 K. Figure 1a shows the real (ϵ') and imaginary (ϵ'') parts of the ϵ spectrum of the LT phase. A large dispersive-shaped line, which was centered at 470 nm with a minimum value at 420 nm and a maximum at 540 nm, was observed in the ϵ' spectrum. The corresponding position in the ϵ'' spectrum showed a strong absorption-shaped peak of $\epsilon'' = 0.68$, which is assigned to the metal-to-metal charge transfer (MM′CT) band of $Fe^{II} \rightarrow Mn^{III}$ (more accurately, CN_{2p_x}, $CN_{2p_y} \rightarrow Mn_{3d_{x^2-y^2}}$, $Mn_{3d_{z^2}}$).[42,44] Table S1 of the Supporting Information lists the other assignments of the small resonance. Figure 1b shows the ϵ' and ϵ'' parts of the ϵ spectrum in the HT phase at 293 K. A dispersive-shaped line, which was centered at 410 nm, was observed. In the corresponding position, an absorption-shaped peak was observed in the ϵ'' spectrum at 410 nm with $\epsilon'' = 0.13$. This peak is assigned to the ligand-to-metal charge transfer (LMCT) transition of $[Fe(CN)_6]^{3-}$ ($^2T_{2g} \rightarrow {}^2T_{1u}$, $CN^- \rightarrow Fe^{III}$).[50]

Photoreversible Changes in the IR Spectra and SQUID Measurement. Because a MM′CT band was observed at 420–540 nm in the ϵ spectrum of the LT phase, the LT phase was irradiated with a CW diode green laser ($h\nu_1$, $\lambda = 532$ nm; Figure 1c). Figure 2 shows the irradiation-time dependence of the IR spectra at 3 K. Before irradiation (Figure 2a, black line), the LT phase possessed a broad peak due to $Mn^{III}-NC-Fe^{II}$ around 2100 cm^{-1}. Irradiating with $h\nu_1$ reduced the $Mn^{III}-NC-Fe^{II}$ peak and created a sharp peak at 2153 cm^{-1}. The latter peak is assigned to the $Mn^{II}-NC-Fe^{III}$ peak, which was also observed in the HT phase (2154 cm^{-1}), although a slight difference existed in the peak shape, as shown in Figure S2 of the Supporting Information. It is concluded that the PI phase after $h\nu_1$ irradiation has a valence state similar to that of the HT phase. Based on the knowledge that a resonance due to the LMCT band was observed at 410 nm in the ϵ spectrum of the HT phase, this PI phase was irradiated with blue light ($h\nu_2$; $\lambda = 410 \pm 30$ nm) from a filtered xenon lamp in order to investigate the photoreversibility. Consequently, the $Mn^{II}-NC-Fe^{III}$ peak decreased and the $Mn^{III}-NC-Fe^{II}$ peak increased, as shown in Figure 2b. Figure 2c plots the peak intensities of $Mn^{III}-NC-Fe^{II}$ versus the irradiation time. This photoreversibility was repeatedly observed.

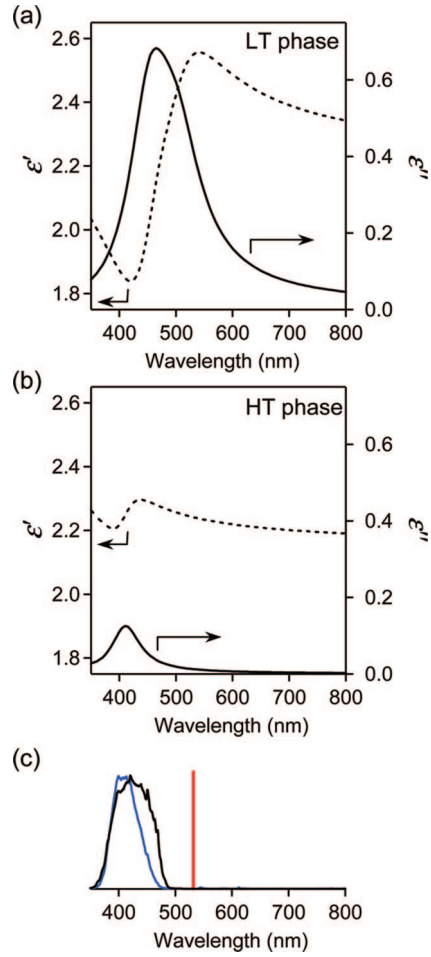

Figure 1. Real (ϵ') and imaginary (ϵ'') parts of the dielectric constant (ϵ) spectra in the (a) LT phase and (b) HT phase of $Rb_{0.88}Mn[Fe(CN)_6]_{0.96}\cdot 0.5H_2O$. Dashed and solid lines represent the ϵ' and ϵ'' parts, respectively. (c) Wavelengths of irradiation lights: $h\nu_1$, $\lambda = 532$ nm (red line); $h\nu_2$, $\lambda = 410 \pm 30$ nm (blue line); $h\nu_3$: $\lambda = 425 \pm 45$ nm (black line).

Next, we measured the photoreversible change in magnetization in situ using SQUID equipment. The field-cooled magnetization curve under an external magnetic field of 200 G showed that the LT phase is a ferromagnet with a Curie temperature (T_C) of 12 K (Figure 3a, closed squares). Upon irradiation with $h\nu_1$ at 3 K, the magnetization value decreased from 5600 to 700 G cm^3 mol^{-1} (Figure 3a, open circles). Successively irradiating the PI phase with $h\nu_2$ increased the magnetization, which reached 4700 G cm^3 mol^{-1} (Figure 3a, closed circles). The inset of Figure 3a shows the magnetic hysteresis curves after irradiation with $h\nu_1$ and $h\nu_2$ lights. The present photoreversibility of the magnetization was repeatedly observed by alternating irradiation with $h\nu_1$ and $h\nu_2$ (Figure 3b).

(50) Schatz, P. N.; McCaffery, A. J.; Suëtaka, W.; Henning, G. N.; Ritchie, A. B.; Stephens, P. J. *J. Chem. Phys.* **1966**, *45*, 722.

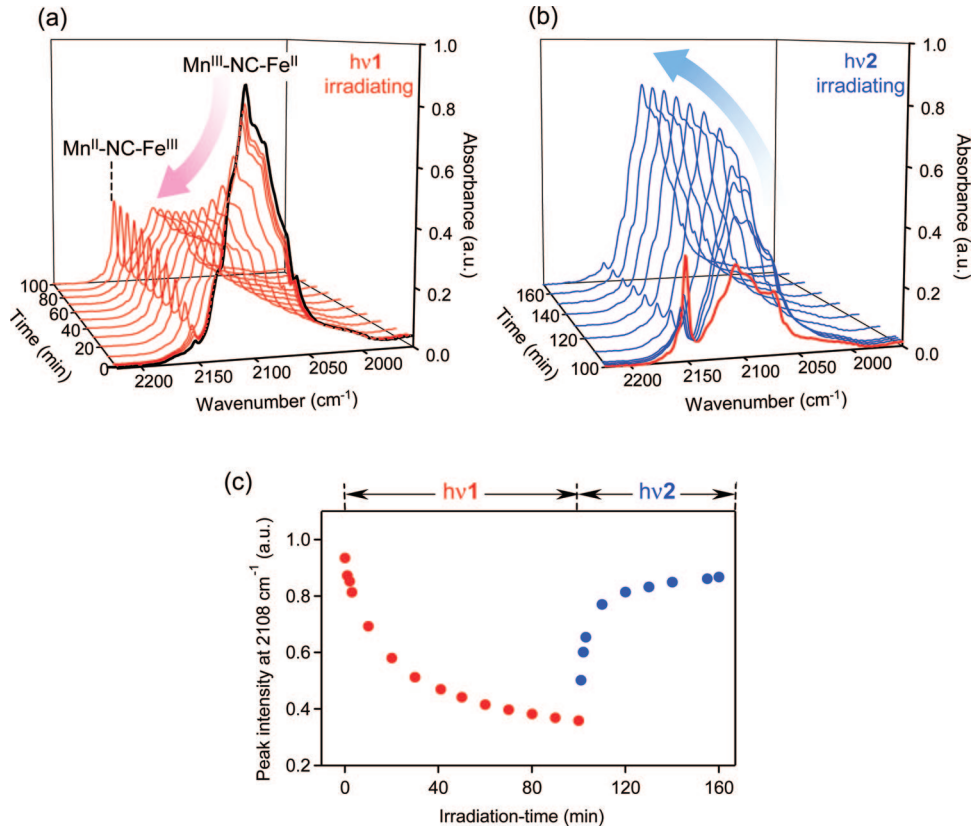

Figure 2. Visible-light-induced reversible change in the IR spectra of $Rb_{0.88}Mn[Fe(CN)_6]_{0.96}\cdot 0.5H_2O$. (a) Irradiation-time dependence of the IR spectra at 3 K by irradiating with $h\nu_1$ (λ = 532 nm). (b) Irradiation-time dependence of the photoreverse process by irradiating with $h\nu_2$ (λ = 410 nm). (c) Peak intensity at 2108 cm^{-1} vs irradiation time upon irradiation with $h\nu_1$ (red circles) and $h\nu_2$ (blue circles).

The magnetization value after irradiation with $h\nu_2$, which is shown as the closed circles in Figure 3a, was smaller than that of the initial value, suggesting that a photoequilibrium state persists. To confirm the photoequilibrium behavior, we investigated the photoeffect of the reverse process, i.e., from the PI phase to the LT phase, using a different light ($h\nu_3$; λ = 425 ± 45 nm; see Figure 1c). Irradiating with $h\nu_3$ increased the magnetization, which reached plateau $M_{h\nu 3}$, as shown in Figure 4. Subsequent irradiation with $h\nu_2$ further increased the magnetization, which reached plateau $M_{h\nu 2}$. This equilibrium behavior is due to a photostationary state between the photodemagnetization (LT → PI phase) and the photoinduced magnetization (PI → LT phase).

3.2. Neutron Powder Diffraction Measurement of $Rb_{0.58}Mn[Fe(CN)_6]_{0.86}\cdot 2.3H_2O$. We performed neutron powder diffraction using an analogue complex, $Rb_{0.58}Mn[Fe(CN)_6]_{0.86}\cdot 2.3H_2O$, to determine the magnetic ordering of the PI phase.

A charge-transfer phase transition was not observed in the IR spectrum of $Rb_{0.58}Mn[Fe(CN)_6]_{0.86}\cdot 2.3H_2O$ when the sample was cooled to 3 K at a rate of –0.5 K min^{-1} (Figure 5a). The $\chi_M^{-1}-T$ plot showed a negative Weiss temperature of –16 K, which was obtained by the least-squares fitting in the temperature region of 150–320 K (Figure S3a of the Supporting Information). The magnetization vs temperature curve under an external field of 10 G exhibited an antiferromagnetic behavior with a Néel temperature (T_N) of 11.5 K (Figure S3b of the Supporting Information). The magnetization vs external magnetic field plots at 2 K showed a linear change (Figure 5b). These magnetic data suggest that, in $Rb^{I}_{0.58}Mn^{II}[Fe^{III}(CN)_6]_{0.86}\cdot 2.3H_2O$, the HT phase is maintained even at low temperature and the HT phase shows antiferromagnetism.

Figure 5c shows the neutron powder pattern for $Rb^{I}_{0.58}Mn^{II}[Fe^{III}(CN)_6]_{0.86}\cdot 2.3H_2O$ at 30 K. Rietveld analysis showed that the crystal structure was tetragonal (*P4/mmm*) with lattice constants of $a = b = 7.424(6)$ Å and $c = 10.51(1)$ Å, which correspond to $a' = b' = 10.499$ Å and $c' = 10.51(1)$ Å in the frame of a cubic lattice (Figure 5c, inset). The interatomic distances of Fe and C in the *ab* plane (Fe–C_{ab}) and along the *c* axis (Fe–C_c) are 1.93(3) and 1.81(4) Å, respectively. The distances of Mn–N_{ab} and Mn–N_c are 2.18(2) and 2.18(4) Å, respectively. Table S2 of the Supporting Information lists the atomic coordinates and occupancy of each atom. Parts a and b of Figure 6 show the neutron powder diffraction patterns at 2 and 30 K and the magnetic Bragg reflections as the difference in the patterns of 2 and 30 K, respectively. Analysis of the magnetic Bragg reflections suggests that this system is a layered antiferromagnet in which the magnetic coupling between the layers is antiferromagnetic. The spin arrangement as shown in Figure 6d is a suitable configuration for the following reason. The electronic state of Mn^{II} is a $3d^5$ high-spin state, and hence, all of the 3d orbitals are magnetic orbitals. In contrast, Fe^{III} is a $3d^5$ low-spin state, and thus, only one of the t_{2g} orbitals becomes a magnetic orbital. Rietveld analysis showed elongation of $Fe(CN)_6$ in the *ab* plane, indicating that the d_{yz} and d_{zx} orbitals are

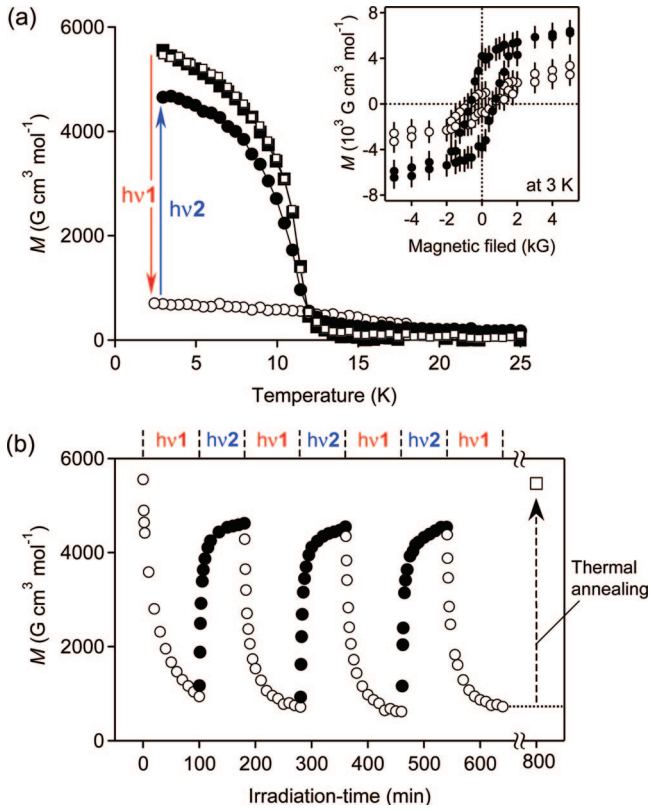

Figure 3. Visible-light-induced reversible photomagnetism in $Rb_{0.88}Mn[Fe(CN)_6]_{0.96}\cdot 0.5H_2O$. (a) Magnetization vs temperature curves at 200 G; before irradiation (■), after $h\nu_1$ ($\lambda = 532$ nm, 30 mW cm^{-2}) irradiation for 100 min (○), after $h\nu_2$ ($\lambda = 410$ nm, 13 mW cm^{-2}) irradiation for 80 min (●), and after thermal annealing treatment of 180 K (□). Inset: Magnetic hysteresis curves at 3 K after irradiation with $h\nu_1$ (○) and $h\nu_2$ (●). (b) Magnetization vs irradiation time plot at 3 K by alternating with $h\nu_1$ (○) and $h\nu_2$ (●) light irradiation and the magnetization value after thermal treatment of 180 K (□).

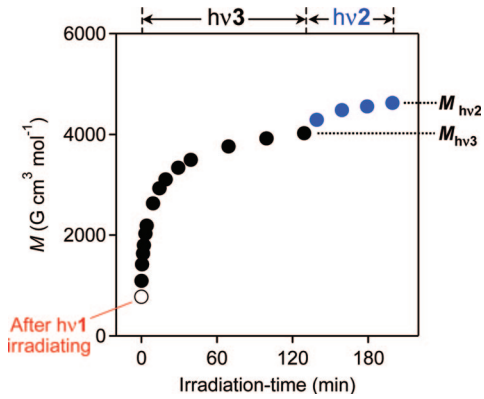

Figure 4. Photostationary state between photodemagnetization and photoinduced magnetization. Magnetization vs irradiation time plot at 3 K upon irradiation with $h\nu_3$ ($\lambda = 425 \pm 45$ nm, 22 mW cm^{-2}) (black circles) and then $h\nu_2$ ($\lambda = 410 \pm 30$ nm, 13 mW cm^{-2}) (blue circles).

more stabilized than the d_{xy} orbital because of back-bonding of the cyanide ligand. Hence, the d_{xy} orbital becomes the magnetic orbital of Fe^{III}. In this case, only the spin configuration shown in Figure 6d can possibly be formed. The stick diagram of Figure 6c, which was calculated by the layered antiferromagnet mentioned above, reproduced the observed data. Because the magnetic ordering of $Rb_{0.58}Mn[Fe(CN)_6]_{0.86}\cdot 2.3H_2O$ is considered to be the same as that of the PI phase in

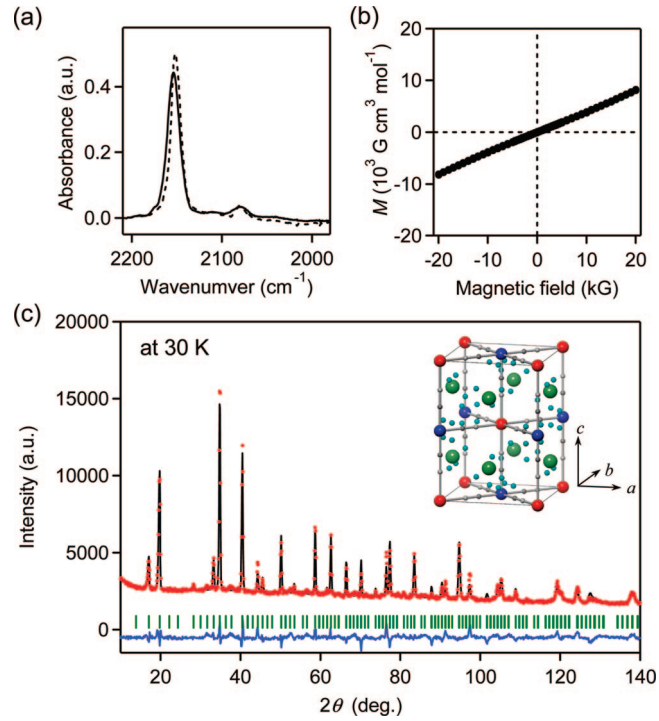

Figure 5. Electronic state, magnetic property, and neutron powder diffraction pattern of $Rb_{0.58}Mn[Fe(CN)_6]_{0.86}\cdot 2.3H_2O$. (a) IR spectra at 300 K (dotted line) and 3 K (solid line). (b) Magnetization as a function of the external magnetic field at 2 K. (c) Neutron powder diffraction pattern at 30 K. The red dots, black line, and blue line are the observed plots, calculated pattern, and their difference, respectively. Green bars represent the calculated positions of the Bragg reflections. Inset: Schematic crystal structure determined by Rietveld analysis at 30 K. Green, red, and blue circles are Rb, Mn, and Fe atoms, respectively. Small dark gray, light gray, and sky blue circles are C, N, and O atoms, respectively. H atoms are omitted for clarity. Table S2 of the Supporting Information lists the atomic coordinates and occupancy.

$Rb_{0.88}Mn[Fe(CN)_6]_{0.96}\cdot 0.5H_2O$, the PI phase should be a layered antiferromagnet.

3.3. Mechanism of Visible-Light-Induced Reversible Photomagnetism. The observed reversible photomagnetic effect can be explained by the scheme shown in Figure 7. Irradiating with $h\nu_1$ excites the MM′CT ($Fe^{II} \rightarrow Mn^{III}$) band, which then excites the LT phase to photoexcited state **I**. Photoexcited state **I** proceeds to the PI phase, which has the same valence state as the HT phase. Thermal energy then suppresses the relaxation of the metastable PI phase to the stable LT phase. In contrast, the excitation of the LMCT ($CN^- \rightarrow Fe^{III}$) band of $[Fe(CN)_6]^{3-}$ by irradiation with $h\nu_2$ excites the PI phase to photoexcited state **II**, which then proceeds to the LT phase. The LT phase is a ferromagnet because of the ferromagnetic coupling between the Mn^{III} ($S = 2$) sites, but the PI phase is an antiferromagnet. Hence, the magnetization value changes by optical switching between the LT and PI phases.

4. Conclusion

In summary, a visible-light-induced reversible photomagnetism between the ferromagnetic and antiferromagnetic phases is observed in a rubidium manganese hexacyanoferrate, $Rb_{0.88}Mn[Fe(CN)_6]_{0.96}\cdot 0.5H_2O$, by alternate irradiation with 532 and 410 nm light. Optical switching from the LT phase to the PI phase occurs through a $Fe^{II} \rightarrow Mn^{III}$ MM′CT

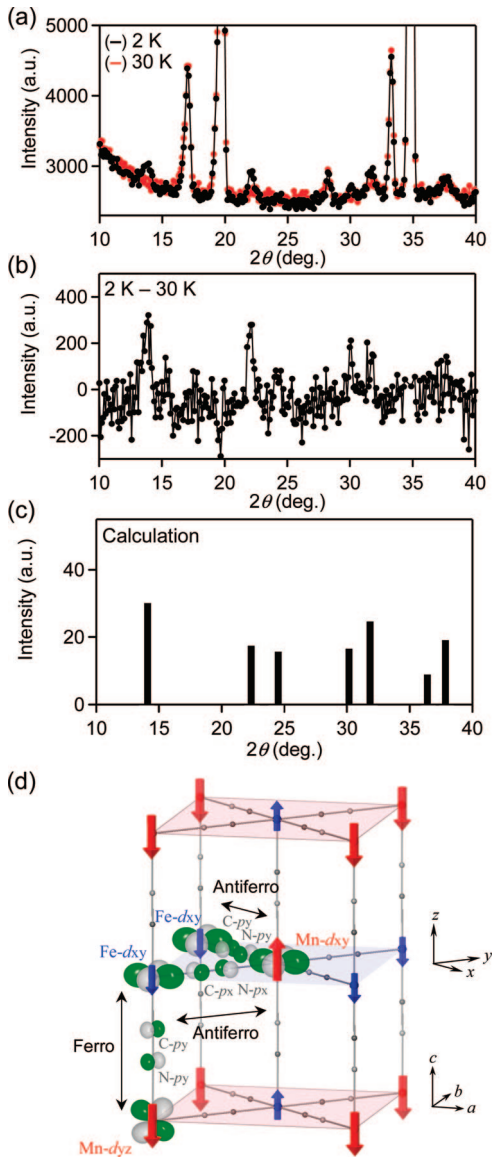

Figure 6. (a) Neutron powder diffraction patterns at 2 K (black line) and 30 K (red line). (b) Magnetic Bragg reflections as the difference in the neutron powder diffraction patterns at 2 and 30 K. (c) Calculated intensities of the magnetic Bragg reflections with an antiferromagnetic spin ordering. (d) Schematic illustration of the spin ordering. Red and blue arrows indicate the spins on Mn^{II} and Fe^{III}, respectively. From the view of the superexchange pathway, an antiferromagnetic coupling operates between Fe d_{xy} and Mn d_{xy} magnetic orbitals in the *xy* (*ab*) plane. In contrast, a ferromagnetic coupling operates between Fe d_{xy} and all of the d orbitals of Mn (here, Mn d_{yz} is depicted) along the *z* (*c*) axis.

transition, causing photodemagnetization. In contrast, the reverse process is caused by an optical transition from the PI phase to the LT phase through a $CN^- \rightarrow Fe^{III}$ LMCT transition. The existence of a photostationary state between

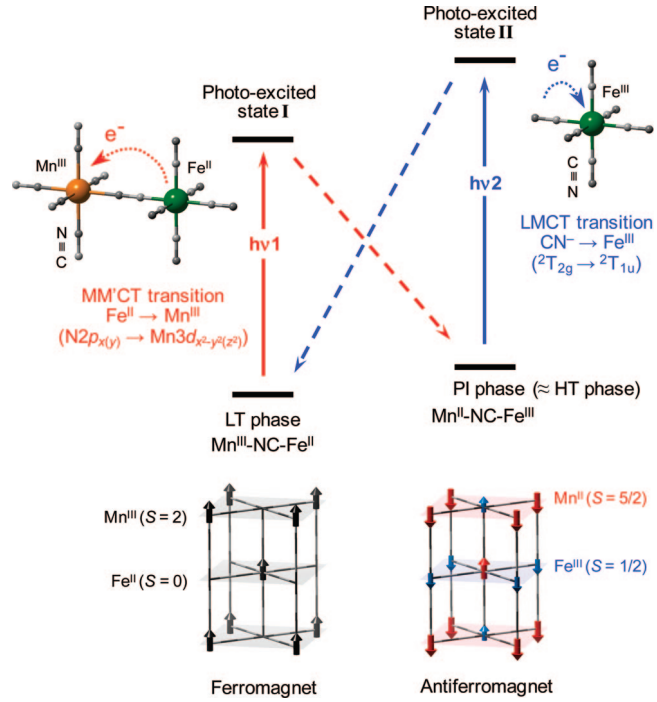

Figure 7. Schematic illustration of the visible-light-induced reversible photomagnetic effect in rubidium manganese hexacyanoferrate. Scheme for reversible charge transfer between $Mn^{III}-NC-Fe^{II}$ and $Mn^{II}-NC-Fe^{III}$ states (upper) and the spin ordering for the LT and PI phases (lower). The LT phase is a ferromagnet because of ferromagnetic coupling between the Mn^{III} sites, whereas the PI phase is an antiferromagnet. Black arrows on the LT phase represent the spins of Mn^{III}. Red and blue arrows on the PI phase indicate the spins of Mn^{II} and Fe^{III}, respectively.

the LT → PI and PI → LT phases is also confirmed by the light source changing experiment. Although photomagnetism has been observed in some compounds, this is the first example of optical switching between a ferromagnet and an antiferromagnet.

Acknowledgment. The authors thank Prof. K. Hashimoto for his helpful discussion. The present research is supported by the Japan Society for the Promotion of Science (JSPS) and a Grant-in-Aid for Scientific Research from the Ministry of Education, Culture, Sports, Science and Technology of Japan and the Yamada Science Foundation.

Supporting Information Available: Information relating to the thermal phase transition, IR spectra, and XRD patterns in the HT and LT regions for $Rb_{0.88}Mn[Fe(CN)_6]_{0.96}\cdot 0.5H_2O$, analysis of the ϵ spectra of $Rb_{0.88}Mn[Fe(CN)_6]_{0.96}\cdot 0.5H_2O$, IR spectra of the HT and PI phases of $Rb_{0.88}Mn[Fe(CN)_6]_{0.96}\cdot 0.5H_2O$, magnetic properties, and Rietveld structural analysis for $Rb_{0.58}Mn[Fe(CN)_6]_{0.86}\cdot 2.3H_2O$. This material is available free of charge via the Internet at http://pubs.acs.org.

CM701873S